THE JOURNAL OF BIOLOGICAL CHEMISTRY
Vol. 277, No. 27, Issue of July 5, pp. 24653–24658, 2002

Printed in U.S.A.

A "Minimal" Sodium Channel Construct Consisting of Ligated S5-P-S6 Segments Forms a Toxin-activatable Ionophore*

Received for publication, December 12, 2001, and in revised form, March 29, 2002
Published, JBC Papers in Press, April 24, 2002, DOI 10.1074/jbc.M111862200

Zhenhui Chen‡, Carmen Alcayaga§, Benjamin A. Suárez-Isla§, Brian O'Rourke, Gordon Tomaselli, and Eduardo Marbán¶

From the Institute of Molecular Cardiobiology, The Johns Hopkins University School of Medicine, Baltimore, Maryland, 21205 and the §Program of Physiology and Biophysics, Institute of Biomedical Sciences, Faculty of Medicine, University of Chile, Santiago 6530499, Chile

The large size (six membrane-spanning repeats in each of four domains) and asymmetric architecture of the voltage-dependent Na^+ channel has hindered determination of its structure. With the goal of determining the minimum structure of the Na^+ channel permeation pathway, we created two stable cell lines expressing the voltage-dependent rat skeletal muscle Na^+ channel (μ1) with a polyhistidine tag on the C terminus (μHis) and pore-only μ1 (μPore) channels with S1–S4 in all domains removed. Both constructs were recognized by a Na^+ channel-specific antibody on a Western blot. μHis channels exhibited the same functional properties as wild-type μ1. In contrast, μPore channels did not conduct Na^+ currents nor did they bind [^{3}H]saxitoxin. Veratridine caused 40 and 54% cell death in μHis- and μPore-expressing cells, respectively. However, veratridine-induced cell death could only be blocked by tetrodotoxin in cells expressing μHis, but not μPore. Furthermore, using a fluorescent Na^+ indicator, we measured changes in intracellular Na^+ induced by veratridine and a brevotoxin analogue, pumiliotoxin. When calibrated to the maximum signal after addition of gramicidin, the maximal percent increases in fluorescence (ΔF) were 35 and 31% in cells expressing μHis and μPore, respectively. Moreover, in the presence of 1 μM tetrodotoxin, ΔF decreased significantly to 10% in μHis- but not in μPore-expressing cells (43%). In conclusion, S5-P-S6 segments of μ1 channels form a toxin-activable ionophore but do not reconstitute the Na^+ channel permeation pathway with full fidelity.

Sodium channels conduct the electrical impulse in excitable tissues and serve as the receptors for many drugs and toxins (1). Their essential functional features include highly selective permeation of Na^+ and voltage-dependent gating (2–5). The principal functional unit of the Na^+ channel is the α subunit, which consists of four internally homologous domains (labeled D*I*–D*IV*),[1] each containing six transmembrane segments (S1–S6) and resembling a single α subunit of a voltage-dependent K^+ channel (6) (Fig. 1*A*). These four homologous domains are pseudosymmetrically arranged around a central pore whose structural constituents determine the selectivity and conductance properties of the channel. While the fourth transmembrane segment S4, studded with positively charged residues, confers voltage-sensitive gating (7), the S5 and S6 segments and the S5-S6 linker or the pore-lining ("P") segment line the permeation pathway. Such a structure, while complex and asymmetrical, hints that essential features of the pore may be separable from those that confer gating.

MacKinnon and coworkers (8) have solved the crystal structure of an inwardly rectifying bacterial K^+ channel (KcsA) channel. This important advance provides a framework for testing hypotheses concerning the pore structure of related channels. With only two transmembrane segments and a P segment in each subunit, KcsA channels function perfectly well as K^+-selective ionophores. Compared with KcsA and other Kir-like channels, voltage-dependent channels, sharing the same transmembrane topology of the core segments, have evolved four additional transmembrane segments (S1–S4) in each domain with S4 responsible for voltage gating and S1–S3 presumably insulating hydrophilic S4 from the lipid bilayer. In this view, the functional pore might be fully encoded by the S5-P-S6 fragments, while the rest of the protein is required only for effecting voltage-dependent conformational changes (Fig. 1*B*). Therefore, it is logical to ask whether a Na^+ channel comprised only of S5-P-S6 from each domain will contain the minimal determinants of a functional pore.

In this study, we stably expressed poly(His)-tagged wild-type and pore-only μ1 channel constructs in mammalian cell lines and characterized them biophysically, biochemically, and functionally. The main goal was to test whether the pore-only μ1 channel is functional as an ionophore and as a high affinity toxin-binding scaffold. Such a reduced construct, if functional, would simplify structural determination of the pore region.

EXPERIMENTAL PROCEDURES

Materials and Chemicals—Materials were from the following sources. Saxitoxin (STX) dihydrochloride was kindly provided by Dr. Sherwood Hall (Federal Drug Administration); [^{3}H]STX was from Amersham Biosciences; *N*-methyl-D-glucamine, veratridine, and tetrodotoxin (TTX) were obtained from Sigma; PbTx-3 (pumiliotoxin) was from Calbiochem; HEK293 cells were from the American Type Culture Collection (Manassas, VA); CoroNa Red sodium indicator and gramicidin A were from Molecular Probes (Eugene, OR); anti-Na^+ channel antibody was purchased from Upstate Biotechnology (Lake Placid, NY); and Geneticin (G418 Sulfate) was from Invitrogen.

* This work was supported by National Institutes of Health Grant RO1 HL52768 (to E. M.). The costs of publication of this article were defrayed in part by the payment of page charges. This article must therefore be hereby marked "*advertisement*" in accordance with 18 U.S.C. Section 1734 solely to indicate this fact.

‡ Recipient of the Michel Mirowski Fellowship from the National Association of Pacing and Electrophysiology (NASPE).

¶ The Michel Mirowski, M.D. Professor of Cardiology of The Johns Hopkins University. To whom correspondence should be addressed: Inst. of Molecular Cardiobiology, The Johns Hopkins University School of Medicine, 720 N. Rutland Ave./Ross 844, Baltimore, MD 21205. Tel.: 410-955-2776; Fax: 410-955-7953; E-mail: marban@jhmi.edu.

[1] The abbreviations used are: D, domain; S, segment; P, pore-lining; TTX, tetrodotoxin; STX, saxitoxin; PbTx-3, pumiliotoxin; MOPS, 4-morpholinepropanesulfonic acid; HEK, human embryonic kidney; IRES, internal ribosomal entry site.

Molecular Biology—A DNA fragment containing a c-Myc epitope and a polyhistidine tag from pCDNA3.1 (Invitrogen) was inserted into the *Xba*I site at the 3′-end of the skeletal muscle Na$^+$ channel (μ1) to generate μ1 His-tagged DNA (μHis). μHis DNA, coupled with a green fluorescent protein reporter gene, was then cloned in a polycistronic IRES vector, allowing independent translation of two separate proteins from a single mRNA. The pore-only μ1 DNA (μPore) was generated by deleting S1–S4 of each domain (Fig. 1, *A* and *C*). Specifically, Leu^{128}–Lys^{228} in domain *I*, Leu^{567}–Leu^{680} in domain *II*, Ile^{1020}–Glu^{1137} in domain *III*, and Phe^{1342}–Leu^{1465} in domain *IV* were deleted by PCR using primers with bases covering regions adjacent to the sections of the channel that were deleted (Stratagene). All constructs were verified by sequencing. For mRNA generation, these constructs were cloned into pSP64T vector, and mRNA was transcribed from the SP6 promoter (Ambion, Inc.)

Cell Biology—All cells were grown in Dulbecco's modified Eagle's medium with 10% (v/v) fetal calf serum, 100 units/ml penicillin, 0.1 mg/ml streptomycin at 37 °C with 5% CO_2. Linearized DNA of μHis and μPore were transfected into HEK293 cells, respectively, using LipofectAMINE Plus Reagent (Invitrogen). Two days after transfection, cells were serially diluted with the addition of 0.5 mg/ml Geneticin to select for transfected cells. Colonies were screened initially by epifluorescence and further characterized by whole-cell current measurements and Western blot analysis. Positive clones were again sorted by green fluorescent protein signals using a FACStar Plus cell sorter. For functional assays, 0.5 million cells were seeded and grown overnight in a 35-mm dish. Veratridine was first dissolved in ethanol at a concentration of 150 mM and then in culture medium. For blocking experiments, cells were incubated with TTX for 1 h before adding veratridine. Cell death was determined by counting the percentage of floating cells and trypsinized attached cells that failed to exclude trypan blue.

Electrophysiology—Patch clamp and two electrode voltage-clamp were performed as described previously (9). All recordings were carried out at room temperature (~21 °C).

Membrane Vesicle Preparation—Cells were washed with cold phosphate-buffered saline, pelleted, resuspended in 1 mM EDTA, 50 mM Tris-Cl (pH = 8.0) with protease inhibitors (Roche Molecular Biochemicals), and homogenized. The homogenate was brought up in a final concentration of 300 mM sucrose, 0.5 mM EDTA, 10 mM Hepes-Tris (pH = 7.5) and homogenized again before centrifuging at 4,000 × *g* for 15 min at 4 °C. The supernatant was retained, and homogenization and centrifugation were repeated on the pellet. The supernatants were then mixed to a final concentration of 0.6 M KCl. The mixture was stirred gently for 30 min at 4 °C before centrifuging at 100,000 × *g* for 1 h. The pellet was resuspended in 300 mM sucrose, 10 mM MOPS-Tris (pH = 7.0) and homogenized using a glass-Teflon homogenizer. Protein concentration was determined by a Lowry assay (10). For rat brain membrane vesicle preparation, rat brains were immersed in cold 20 mM MOPS-Tris (pH = 7.4), homogenized using a glass-Teflon homogenizer, and then subjected to the previously described cell membrane vesicle isolation protocol. Normally one rat brain yields about 80 mg of total membrane protein.

STX Binding Assay—The [^{3}H]STX binding assay was performed as described previously by Vélez *et al.* (11). 250 μg of membrane vesicles were incubated on ice for 1 h with buffer containing 2.5 nM [^{3}H]STX, 30 mM choline chloride, 10 mM Hepes-Tris, pH 7.4, and a range of cold STX from a concentration of 0 to a maximum of 4 μM in a 250-μl reaction volume. Free [^{3}H]STX was removed by passing each reaction mixture through a glass filter. The filter was washed twice and counted using a scintillation counter.

Fluorescent Indicator Loading and Microfluorometry—For optimal dye loading, cells were incubated with 1 μM CoroNa Red Na$^+$ indicator (from a freshly dissolved 1 mM stock Me_2SO solution, Molecular Probes) in 140 mM NaCl, 5 mM KCl, 1 mM $MgCl_2$, 1 mM $CaCl_2$, 10 mM glucose, pH 7.4 at 37 °C for 2 h.

Cells were plated on 15-mm glass coverslips and mounted on a perfusion chamber (Warner Instruments, PH4) that was placed on the stage of a Nikon Diaphot inverted fluorescence microscope. A 20× Nikon oil immersion lens was used, and all experiments were done at room temperature. The fluorescence cube in the microscope consisted of a 540 ± 15 nm excitation filter, a 565LP dichroic mirror, and a 620 ± 30 nm emission filter. A 12-bit monochrome cooled CCD camera (5 MHz readout rate, MicroMax, Princeton Instruments) was used to collect 650 × 514 pixel 16-bit grayscale images once every minute with either a 100- or 200-ms exposure time.

Experiments were performed during continuous perfusion of buffers and drugs at 0.6–1.0 ml/min. A run was initiated after a stable fluorescence signal was obtained during perfusion of control solution containing 140 mM NaCl, 5 mM KCl, 1 mM $MgCl_2$, 1 mM $CaCl_2$, 10 mM glucose, pH 7.4. At least 10 images were obtained in each condition. Addition of PbTx-3, an analogue of brevotoxin, and veratridine elicited a slow increase of fluorescence that usually reached steady state within 10–15 min. Normally only one addition of toxin could be done per run. The chamber was then perfused with control solution to dilute the added toxin, and the calibration sequence was initiated. In this case, perfusion was interrupted, and 1 ml of 2 μM gramicidin dissolved in control solution was directly added to the chamber. After development of maximal fluorescence, typically 6–10 min, perfusion was restarted, and the calibration sequence was completed by the consecutive addition of buffers containing different sodium concentrations.

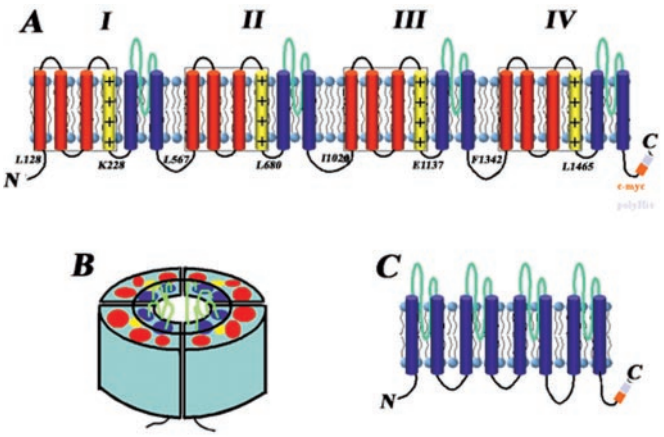

FIG. 1. **Schematic depictions of the Na$^+$ channel α subunit.** *A*, transmembrane topology of the N$^+$ channel. The *boxes* enclose the S1–S4 segments that were deleted to generate the μPore channel. The amino acids of the start of S1 and the end of S4 in each domain are indicated. *B*, schematic of the folding of the Na$^+$ channel around the ion-selective pore. The *ring* highlights the putative channel pore-lining segments. *C*, transmembrane topology of the μPore Na$^+$ channel where S1–S4 segments were deleted in all domains.

Data Analysis—At least five regions of interest covering all the cells were measured in each experiment. Average fluorescence intensity of each region of interest was analyzed by ImageJ (rsb.info.nih.gov/ij/). The percent changes for fluorescence signal, corresponding to the intracellular Na$^+$ changes, were calibrated with gramicidin and calculated using the following formula: $(F - F_{min})/(F_{max} - F_{min}) \times 100\%$, where F is the fluorescence signal, F_{min} is the control signal in normal 140 mM Na$^+$ buffer, and F_{max} is the maximum signal in the presence of gramicidin. At least five points in the plateau were averaged for each treatment. Data were further analyzed and plotted using Origin (Microcal Software, Inc.)

RESULTS

Channel Protein Expression—We created two HEK293 stable cell lines expressing either wild-type μ1 channels with a c-Myc epitope and a polyhistidine (μHis) tag fused to the C terminus or pore-only μ1 (μPore) channels with S1–S4 in all domains removed (Fig. 1*C*). The stably transfected cells all had a normal morphology under basal conditions. Membrane vesicles prepared from both cell lines were recognized by a Na$^+$ channel-specific antibody directed to the retained *III-IV* interdomain linker (SP19). μHis channels, with a calculated molecular mass of 212 kDa, ran at 240 kDa, while μPore, with a calculated molecular weight of 159 kDa, ran at 210 kDa on a Western blot (Fig. 2). Antibodies raised to the c-Myc and poly-(His) tags both recognized μPore and μHis channels (data not shown), indicating that the entire constructs were faithfully expressed. Using a polycistronic IRES vector, we found that the reporter green fluorescent protein and the channel construct were independently expressed and co-localized. In cells expressing either μHis or μPore channels, confocal microscopy indicated that the green fluorescent protein signals were detected at the cell surface membrane (data not shown). These results indicated that μPore channels were expressed at the surface membrane.

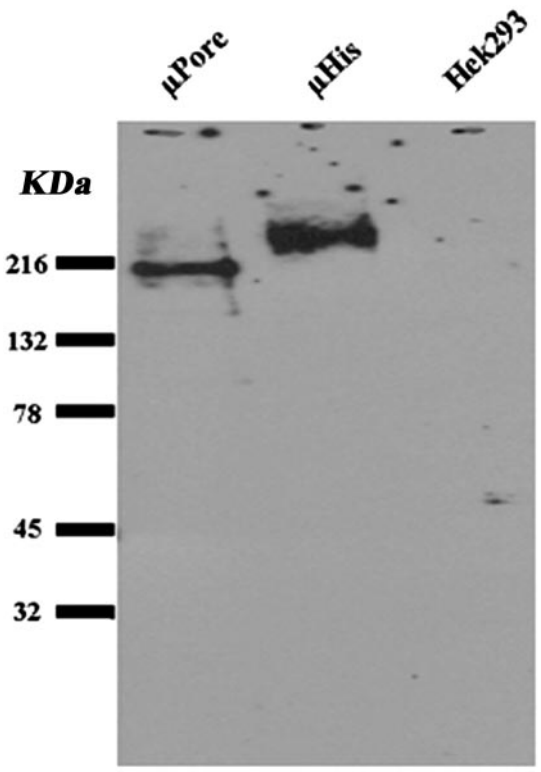

FIG. 2. **Immunoblot analysis.** A Na$^+$ channel-specific antibody that recognizes an epitope in the interdomain *III-IV* linker binds to both μPore and μHis channels. Membrane vesicles were prepared as described under "Experimental Procedures." 10 μg of total membrane proteins for μPore, μHis, and HEK293 cells were subjected to SDS-PAGE (4–15% gradient) and immunoblotting with an anti-Na$^+$ channel polyclonal antibody.

Channel Activity—Channel activity of the μHis and μPore channels was functionally characterized using the patch clamp technique. Whole-cell currents from cells stably expressing μHis channels exhibit the same electrophysiological properties as wild-type μ1 channels (Fig. 3*A*), indicating they are fully functional. In contrast, μPore failed to conduct measurable time-dependent, Na$^+$-selective currents despite expression of the protein (Fig. 3*B*). In addition, no currents were observed in either mRNA-injected *Xenopus* oocytes or transiently transfected HEK293 cells (data not shown). One explanation is that μPore channels may not be able to fold properly to form an ionophore; alternatively, μPore channels may generate a pore that favors a closed conformation. Since the voltage-sensing S4 segments are not present in μPore channels, voltage changes may not be able to generate conformational changes necessary to open μPore channels. Nevertheless, we explored the possibility that such channels might retain toxin sensitivity.

STX Binding Assay—TTX and STX block the Na$^+$ channels at neurotoxin receptor site 1, which is localized near the extracellular opening of the pore. High affinity STX binding requires a highly stereotypical three-dimensional structure with crucial contributions from numerous pore residues present in the extracellular linkers, including those from the P segments (12–16). Thus, preservation of STX binding could be considered as evidence of proper processing and folding of μPore channels. We performed STX binding assays on membrane vesicles of rat brain, stable cell lines expressing μ1 and μPore channels, and non-transfected HEK293 cells. Control HEK293 cells did not bind STX. In contrast, rat brain membrane vesicles exhibited strong [^{3}H]STX binding with a total concentration of the binding sites (B_{max}) of 0.86 pmol of [^{3}H]STX binding/mg of total membrane protein in agreement with previous reports (17, 18).

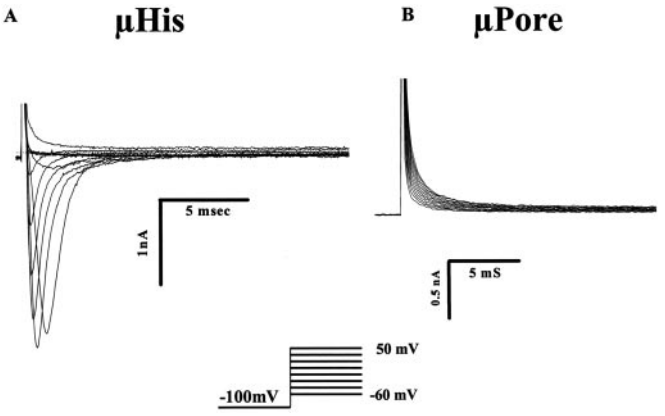

FIG. 3. **Whole-cell Na$^+$ current recordings.** Shown are currents elicited by a family of depolarizing voltage steps from a holding potential of −100 mV to test voltages of −60 to +50 mV in increments of 10 mV. In *A*, HEK293 cells expressing μHis channels exhibit normal currents, while in *B*, cells expressing μPore channels did not have any time- or voltage-dependent currents.

Membrane vesicles containing μ1 channels exhibited specific [^{3}H]STX binding with a B_{max} of 0.46 pmol/mg of protein (Fig. 4*A*). However, the [^{3}H]STX binding signal of membrane vesicles containing μPore channels was indistinguishable from background. In addition, in [^{3}H]STX displacement assays using non-radioactive STX, rat brain membrane vesicles and membrane vesicles containing μ1 channels exhibited specific [^{3}H]STX binding (Fig. 4*B*), but again μPore channels did not exhibit any [^{3}H]STX displacement. These data suggest that μPore channels did not preserve a Na$^+$ channel structure that specifically binds to STX. Nevertheless, we tested whether μPore channels remained sensitive to other Na$^+$ channel toxins that bound to sites distinct from the STX binding site.

Veratridine-induced Cell Death—Veratridine causes persistent opening of Na$^+$ channels and elevates intracellular Na$^+$ concentration, which perturbs ion homeostasis sufficiently in neurons and astroglia to trigger cell death (19, 20). If our cells contained any toxin-activable Na$^+$ channels, they may likewise die during exposure to veratridine. Thus, we determined whether veratridine affected cell viability in our stable cell lines.

Control (non-transfected) HEK293 cells and cells expressing μPore and μHis channels were incubated with various concentrations of veratridine for 20 h at 37 °C, 5% CO_2. Cell death was assayed by the inability to exclude trypan blue (Fig. 5*A*). In the absence of veratridine, none of the three cell lines exhibited measurable cell death. However, at veratridine concentrations of 200 μM or higher, cells expressing μHis and μPore channels showed significantly more cell death than did control HEK293 cells. At 225 μM veratridine, in control HEK293 cells, only 16% of cells were killed, but 40 and 54% of cells expressing μHis and μPore channels died, respectively (Fig. 5*B*). This effect was specific as the proapoptotic agents staurosporine and etoposide did not cause more cell death in μPore cells than in μHis cells (data not shown).

When STX/TTX binding is intact, TTX potently blocks the action of site 2 toxins. Therefore, TTX should block the veratridine-induced cell death in μHis cells (19) but not in μPore cells if μPore channels do not bind TTX. Under the same conditions, veratridine-induced cell death was significantly decreased in cells expressing μHis in 50 and 200 μM TTX (Fig. 5*B*), confirming that TTX indeed blocked Na$^+$ influx through μHis channels induced by veratridine. In addition, no significant changes were observed in control HEK293 cells (15 and 12% of cell death in 50 and 200 μM TTX, respectively). However, TTX did not reduce veratridine-induced cell death in cells

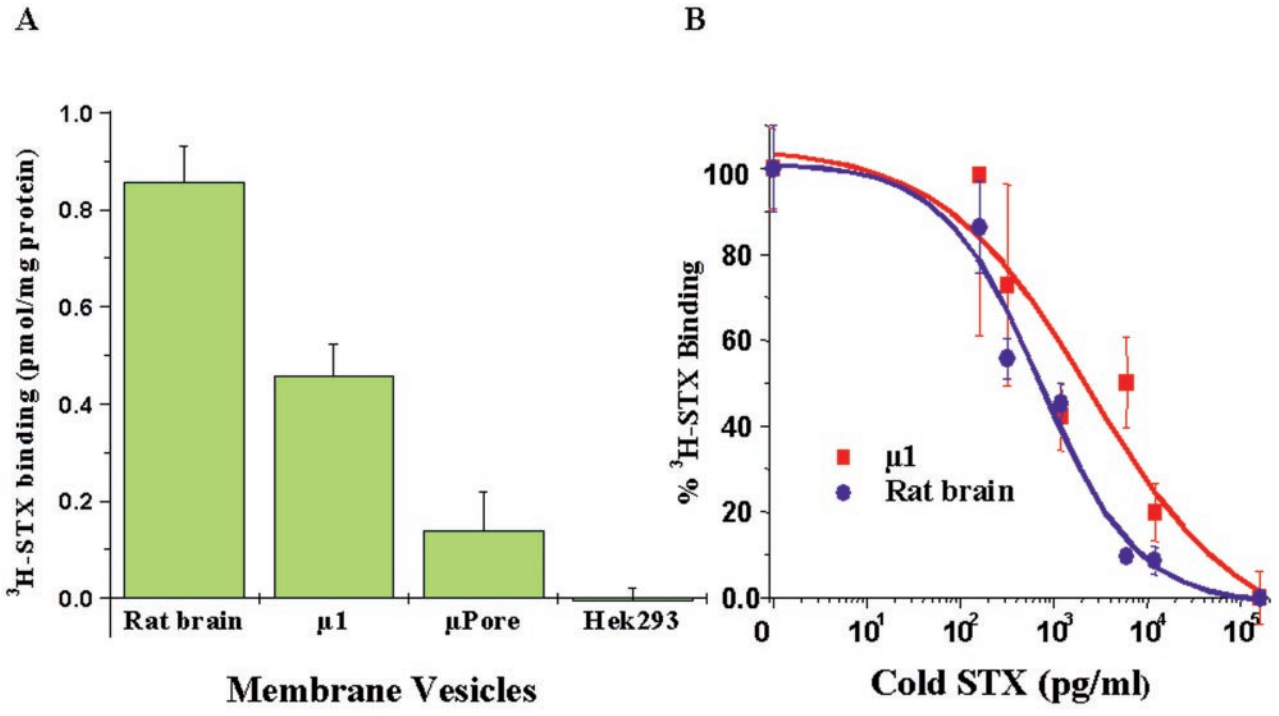

FIG. 4. **[^{3}H]STX binding in membrane vesicles of rat brain, native HEK293 cells, and cells expressing µ1His and µPore channels.** *A*, equilibrium binding of 2.5 nM [^{3}H]STX binding to membrane vesicles as described under "Experimental Procedures" (n = 3). *B*, [^{3}H]STX displacement by increasing concentrations of cold STX. In contrast to rat brain and µ1His-containing vesicles, µPore (n = 3) did not exhibit any [^{3}H]STX displacement.

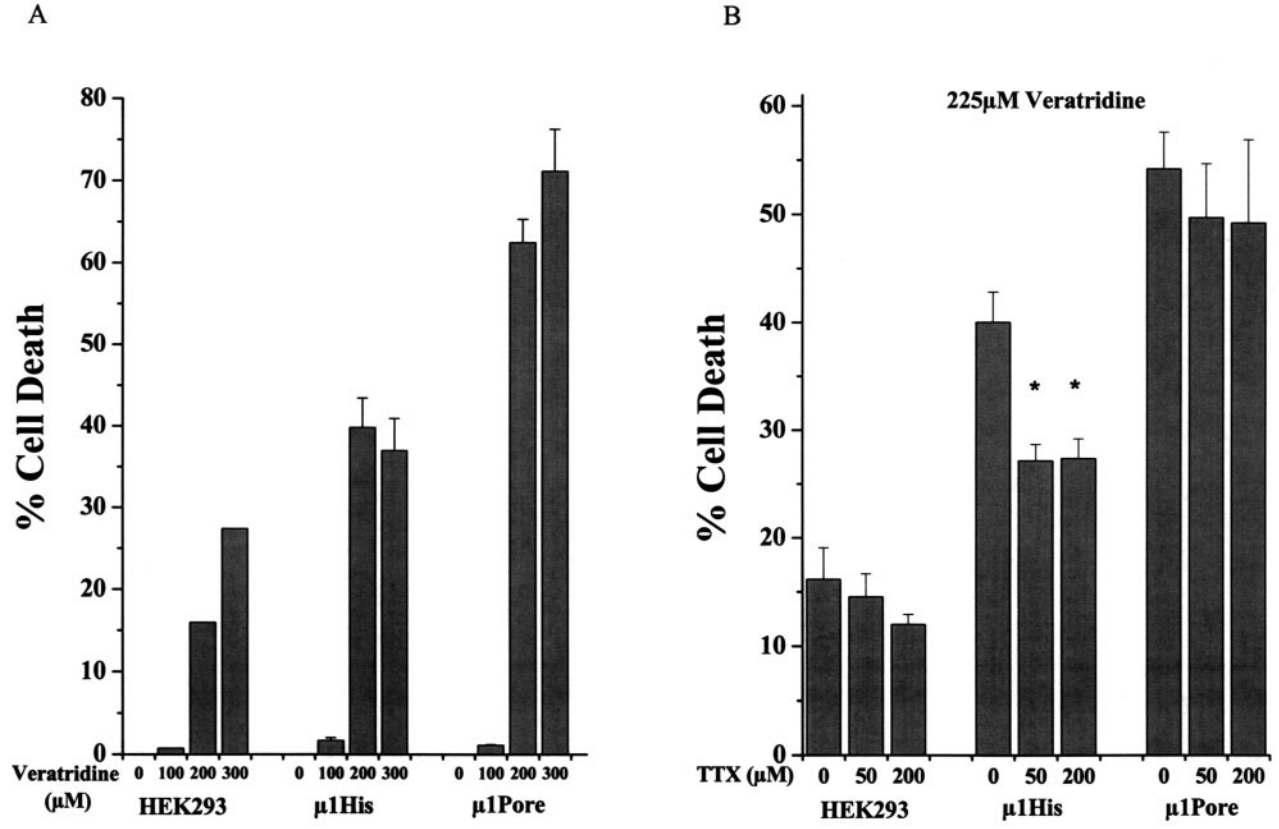

FIG. 5. **Veratridine induced cell death.** *A*, in normal Dulbecco's modified Eagle's medium, veratridine reduced cell survival in µ1His- and µPore-expressing HEK293 cells as assessed by failure to exclude trypan blue. *B*, veratridine-induced cell death was partial blocked by TTX in cells expressing µ1His channels but not µPore channels (n = 4; *, $p < 0.01$, one-way analysis of variance).

expressing µPore channels, with cell death rates of 50 and 49% in 50 and 200 µM TTX, respectively (Fig. 5*B*). Therefore, while blocking Na^+ channels and antagonizing veratridine-induced cell death in µHis cells, TTX failed to block veratridine-induced cell death in µPore cells. Taken together, the findings were consistent with the idea that µPore channels retain veratridine

sensitivity but lose the ability to bind TTX and STX. To obtain additional independent evidence for a toxin-recruitable ionophore, we measured intracellular Na^+ in cells expressing μHis and μPore channels.

Toxin-induced Na^+ Influx—If a μPore channel forms a veratridine-recruitable ionophore, one would expect an acute increase of Na^+ influx when μPore is activated by veratridine. When veratridine alone was applied to cells expressing μPore channels, there was no consistent activation of Na^+-selective currents in patch clamp recordings (data not shown), perhaps due to the small density and time-independent nature of the currents. The lack of TTX sensitivity also made it impossible to use toxin sensitivity as a tool to specifically isolate the current. Therefore, we developed an alternative strategy to assay intracellular Na^+ changes in response to the opening of channels induced by toxin treatment. CoroNa Red, a Na^+-specific fluorescent dye, exhibits sensitive responses to Na^+ concentration in the thin layer of fluid at the surface of large airways (21). Here we used CoroNa Red Na^+ indicator to measure intracellular Na^+ changes generated by Na^+ influx through Na^+ channels elicited by activating toxins.

The intracellular Na^+ concentration changes were detected by changes in the CoroNa Red fluorescence using a CCD camera. These signals were normalized to the percent increase in fluorescence (ΔF) relative to the maximum signal after the addition of gramicidin when intracellular and extracellular Na^+ had presumably reached equilibrium. In all experiments, gramicidin elicited an average 2.6-fold increase over the background signal. Veratridine alone did not induce a significant increase in ΔF in either μHis or μPore cells at least in the short term (over ~30 min, data not shown). Therefore, we used a combination of PbTx-3 and veratridine to activate these channels, exploiting the fact that PbTx-3 may allosterically stimulate veratridine-induced Na^+ flux. Fig. 6*A* shows representative data for μPore and μHis channels with summary plots shown in Fig. 6*B*. In control HEK293 cells, PbTx-3 and veratridine only generate an average of a 2.5% increase in ΔF (Fig. 6*B*). In cells expressing either μHis or μPore channels, addition of the mixture of PbTx-3 and veratridine elicited a ΔF increase of 35 and 31%, respectively, suggesting that there was a significant increase of intracellular Na^+ due to Na^+ influx through toxin-activated μHis or μPore channels. Furthermore, preincubation of 1 μM TTX significantly decreased ΔF in μHis cells but not in μPore cells. Thus, PbTx-3 and veratridine activated both μPore and μHis channels and resulted in Na^+ influx through the activated channel pore. The Na^+ influx in activated μPore channels is resistant to block by TTX, further confirming the insensitivity of μPore channels to TTX.

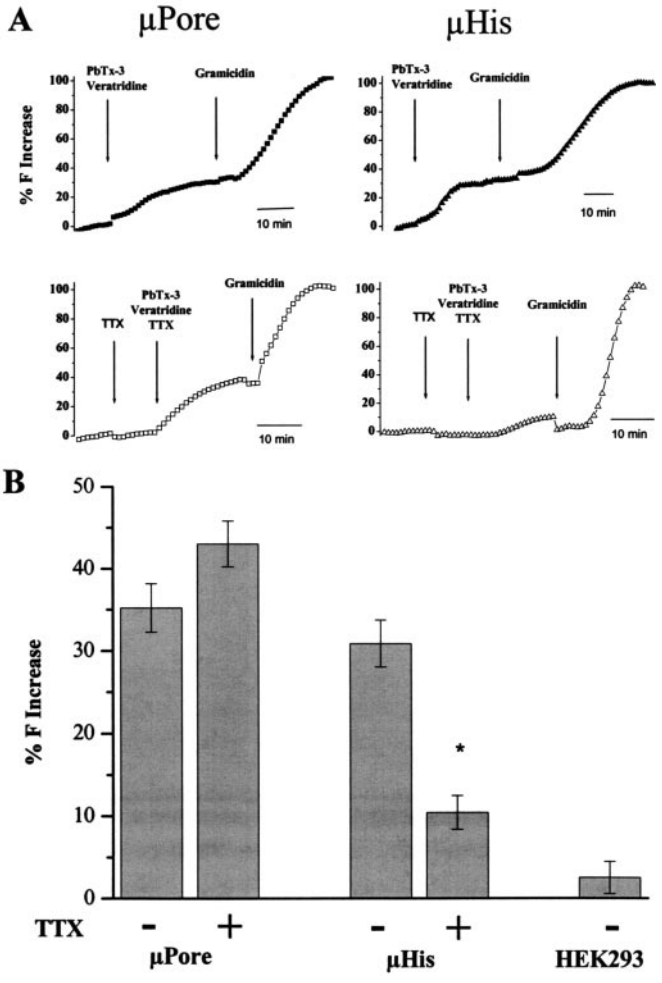

FIG. 6. **Toxins induced Na^+ influx.** *A*, representative experiments of the percent change in fluorescence in HEK293 cells loaded with CoroNa Red expressing μ1His and μPore channels when exposed to different toxins. *B*, summary data plotting the change in fluorescence when cells were exposed to 112 nM PbTx-3 and 150 μM veratridine with or without preincubation of 1 μM TTX ($n = 4$; regions of interest > 25; *, $p < 0.001$).

DISCUSSION

In a quest for a "minimal" Na^+ channel structure, we trimmed the channels of all but those core segments that would be absolutely required for permeation. Based on the structure of KcsA and other Kir family K^+ channels, we reasoned that the S5-P-S6 segments of a voltage-dependent Na^+ channel might retain some aspects of a functional pore. Through biochemical and physiological characterizations, we found that S5-P-S6 segments of μ1 channels do form functional ionophores, albeit ones that lack full fidelity when compared with the parent channels. Key structural motifs of Na^+ channels are missing in μPore channels in that they fail to bind TTX or STX functionally and biochemically. Nevertheless, μPore ionophores can be activated by the Na^+ channel toxins veratridine and PbTx-3 as gauged by Na^+ fluorescence measurements and cell viability assays.

The following considerations support the notion that the fluorescence increases induced by PbTx-3 reflect the stimulation of Na^+ influx through Na^+ channels. First, *in situ* calibration curves (not shown) indicated that CoroNa Red can track sodium very specifically regardless of whether the remaining salt in the solution is *N*-methyl-D-glucamine chloride or KCl. Second, we also have excluded potassium as a measurable interfering cation from examination of the *in situ* calibration curves that show that CoroNa Red fluorescence *decreases* in the presence of high K^+ concentrations (NaCl/KCl buffers) as compared with the values obtained in the absence of K^+ at the same Na^+ concentration (*i.e.* in NaCl/*N*-methyl-D-glucamine buffers). Due to the dye structure, the coordination of negative ions should be excluded from the crown moiety that coordinates sodium. The same would be the case for divalent cations, although there could be some competition as CoroNa Red is derived from EDTA-like moieties. Third, the fluxes were only seen when PbTx-3 was added to cells expressing Na^+ channels. The signals were not observed after high K^+ depolarization of HEK293 cells expressing Na^+ channels or in control HEK cells with any of the treatments. The fluxes were also detected when cells expressing Na^+ channels were exposed simultaneously to PbTx-3 and veratridine dissolved in a 45 mM K^+ buffer, but they were similar to those in PbTx-3 and veratridine in a normal low K^+ buffer for both μpore and μHis cells. This treatment did not induce a fluorescence increase in control

HEK293 cells, indicating that, during toxin activation, the fluxes are not affected in a measurable way by changes in the electrochemical gradient for potassium. If K^+ efflux were to co-exist in μPore but not in μHis cells, a measurable difference would have been expected in the fluorescence changes. Finally, during toxin activation in normal 140 mM Na^+ buffer, potassium would be leaking out, and therefore the proportion of K^+-dye complexes should, if anything, decrease, producing a decrease in F if K^+ were indeed a serious contaminant. For these reasons, we believe that the toxin-activated fluorescence signals reflect Na^+ flux through Na^+ channels.

Gating of the μPore Channel—The pore of Na^+ channels exhibits a high degree of conformational flexibility and is involved in channel gating. The domain *III-IV* linker of Na^+ channels is a prime determinant of rapid inactivation (7, 22, 23), while the external pore has been linked to slow inactivation (24–26). We hypothesized that the inactivation mechanisms should be preserved in μPore channels as these structural elements are still intact. Indeed, like wild-type Na^+ channels, μPore channels predominately are in closed or inactivated conformations at rest; otherwise, persistent Na^+ influx at rest might be expected to kill cells expressing μPore. Since the voltage sensor is not present, μPore channels cannot be activated by depolarization. However, non-voltage-dependent activation appears to exist in μPore channels. Our results indicate that μPore channels can be activated by Na^+ channel-opening toxins.

Veratridine and PbTx-3 Mechanisms—Veratridine and PbTx-3 are Na^+ channel openers that bind to site 2 and site 5, respectively, on the α subunit of the Na^+ channel (27). Site 2 neurotoxins, including the alkaloids batrachotoxin, veratridine, aconitine, and grayanotoxin, cause persistent activation of Na^+ channels (28, 29). Studies have shown that veratridine and batrachotoxin share a common binding site in D*I*-S6 and D*IV*-S6 (30, 31). In wild-type channels, veratridine binds to open Na^+ channels (32), blocking inactivation, shifting the voltage dependence of activation to more negative membrane potentials, and reducing selectivity. TTX and STX potently counteract the action of veratridine. Site 5 toxins brevotoxin and PbTx-3, lipid-soluble polyethers, bind to a receptor site located near the transmembrane interface between D*I* and D*IV* near the extracellular side of the D*IV*-S5 segment and the extracellular end of the D*I*-S6 segment of the α subunit (33, 34). This interaction causes a shift in the voltage dependence of channel activation to more negative potentials and inhibits channel inactivation. In addition, the oxygen-rich nature of the brevotoxin backbone interacts with the channel in a manner that stabilizes the open configuration (35). Moreover, site 2 and site 5 lipid-soluble toxins are allosteric modulators of channel function. PbTx-3 allosterically stimulates Na^+ influx generated by site 2 toxins including veratridine and batrachotoxin (36, 37). As segments S5 and S6 are preserved in the μPore construct, the binding sites of veratridine and PbTx-3 might still be intact on μPore channels. Our functional data showed that the interactions of veratridine and PbTx-3 on μPore channel resulted in activation of the ionophore in a non-voltage-dependent fashion.

Conclusions—In an effort to define the minimal structure required to create a functional Na^+ channel pore, we have found that the S5-P-S6 segments of the μ1 Na^+ channel suffice to form a toxin-activable ionophore. Unfortunately, the reduced construct does not provide a compelling platform for further protein purification and structure prediction as it does not retain key biochemical markers (*viz.* STX binding) that would enable tracking of the protein during enrichment and purification. Nevertheless, our observations are conceptually valuable as they identify the minimal determinants for two key features of pore function (Na^+ flux and toxin activation).

REFERENCES

1. Hille, B. (1992) *Ionic Channels of Excitable Membranes*, 2nd Ed., Sinauer Associates, Sunderland, MA
2. Marbán, E., Yamagishi, T., and Tomaselli, G. F. (1998) *J. Physiol.* **508,** 647–657
3. Armstrong, C. M., and Hille, B. (1998) *Neuron* **20,** 371–380
4. Catterall, W. A. (2000) *Neuron* **26,** 13–25
5. Fozzard, H., and Hanck, D. (1996) *Physiol. Rev.* **76,** 887–926
6. Noda, M., Shimizu, S., Tanabe, T., Takai, T., Kayano, T., Ikeda, T., Takahashi, H., Nakayama, H., Kanaoka, Y., Minamino, N., Kangawa, K., Matsuo, H., Raftery, M., Hirose, T., Inayama, S., Hayashida, H., Miyata, T., and Numa, S. (1984) *Nature* **312,** 121–127
7. Stühmer, W., Conti, F., Suzuki, H., Wang, X. D., Noda, M., Yahagi, N., Kubo, H., and Numa, S. (1989) *Nature* **339,** 597–603
8. Doyle, D. A., Cabral, J. M., Pfuetzner, R. A., Kuo, A., Gulbis, J. M., Cohen, S. L., Chait, B. T., and MacKinnon, R. (1998) *Science* **280,** 69–77
9. Chen, Z., Ong, B. H., Kambouris, N. G., Marbán, E., Tomaselli, G. F., and Balser, J. R. (2000) *J. Physiol.* **524,** 37–49
10. Lowry, O. H., Rosebrough, N. J., Farr, A. L., and Randall, R. J. (1951) *J. Biol. Chem.* **193,** 265–275
11. Velez, P., Sierralta, J., Alcayaga, C., Fonseca, M., Loyola, H., Johns, D. C., Tomaselli, G. F., Marbán, E., and Suárez-Isla, B. A. (2001) *Toxicon* **39,** 929–935
12. Satin, J., Kyle, J. W., Chen, M., Bell, P., Cribbs, L. L., Fozzard, H. A., and Rogart, R. B. (1992) *Science* **256,** 1202–1205
13. Backx, P. H., Yue, D. T., Lawrence, J. H., Marbán, E., and Tomaselli, G. F (1992) *Science* **257,** 248–251
14. Chiamvimonvat, N., Perez-Garcia, M. T., Ranjan, R., Marbán, E., and Tomaselli, G. F. (1996) *Neuron* **16,** 1037–1047
15. Lipkind, G., and Fozzard, H. A (1994) *Biophys. J.* **66,** 1–13
16. Terlau, H., Heinemann, S. H., Stühmer, W., Pusch, M., Conti, F., Imoto, K., and Numa, S. (1991) *FEBS Lett.* **293,** 93–96
17. Yotsu-Yamashita, M., Nishimori, K., Nitanai, Y., Isemura, M., Sugimoto, A., and Yasumoto, T. (2000) *Biochem. Biophys. Res. Commun.* **267,** 403–412
18. Doyle, D. D., Guo, Y., Lustig, S. L., Satin, J., Rogart, R. B., and Fozzard, H. A. (1993) *J. Gen. Physiol.* **101,** 153–182
19. Takahashi, S., Shibata, M., and Fukuuchi, Y. (1999) *Eur. J. Pharmacol.* **372,** 297–304
20. Takahashi, S., Shibata, M., Gotoh, J., and Fukuuchi, Y. (2000) *Eur. J. Pharmacol.* **408,** 127–135
21. Jayaraman, S., Song, Y., Vetrivel, L., Shankar, L., and Verkman, A. S. (2001) *J. Clin. Investig.* **107,** 317–324
22. Moorman, J. R., Kirsch, G. E., Brown, A. M., and Joho, R. H. (1990) *Science* **250,** 688–691
23. West, J., Patton, D. E., Scheuer, T., Wang, Y., Goldin, A. L., and Catterall, W. A. (1992) *Proc. Natl. Acad. Sci. U. S. A.* **89,** 10910–10914
24. Tomaselli, G. F., Chiamvimonvat, N., Nuss, H. B., Balser, J. R., Perez-Garcia, M. T., Xu, R. H., Orias, D. W., Backx, P. H., and Marbán, E. (1995) *Biophys. J.* **68,** 1814–1827
25. Balser, J. R., Nuss, H. B., Chiamvimonvat, N., Perez-Garcia, M. T., Marbán, E., and Tomaselli, G. F. (1996) *J. Physiol.* **494,** 431–442
26. Benitah, J. P., Chen, Z., Balser, J. R., Tomaselli, G. F., and Marbán, E. (1999) *J. Neurosci.* **19,** 1577–1585
27. Catterall, W. A. (1980) *Annu. Rev. Pharmacol. Toxicol.* **20,** 15–43
28. Khodorov, B. I. (1985) *Prog. Biophys. Mol. Biol.* **45,** 57–148
29. Sutro, J. B. (1986) *J. Gen. Physiol.* **87,** 1–24
30. Linford, N. J., Cantrell, A. R., Qu, Y., Scheuer, T., and Catterall, W. A. (1998) *Proc. Natl. Acad. Sci. U. S. A.* **95,** 13947–13952
31. Wang, S. Y., and Wang, G. K. (1999) *Biophys. J.* **76,** 3141–3149
32. Barnes, S., and Hille, B. (1988) *J. Gen. Physiol.* **91,** 421–443
33. Trainer, V. L., Thomsen, W. J., Catterall, W. A., and Baden, D. G. (1991) *Mol. Pharmacol.* **40,** 988–994
34. Trainer, V. L., Baden, D. G., and Catterall, W. A. (1994) *J. Biol. Chem.* **269,** 19904–19909
35. Jeglitsch, G., Rein, K., Baden, D. G., and Adams, D. J. (1998) *J. Pharmacol. Exp. Ther.* **284,** 516–525
36. Sharkey, R. G., Jover, E., Couraud, F., Baden, D. G., and Catterall, W. A. (1987) *Mol. Pharmacol.* **31,** 273–278
37. Wada, A., Uezono, Y., Arita, M., Yuhi, T., Kobayashi, H., Yanagihara, N., and Izumi, F. (1992) *J. Pharmacol. Exp. Ther.* **263,** 1347–1351

A ''Minimal'' Sodium Channel Construct Consisting of Ligated S5-P-S6 Segments Forms a Toxin-activatable Ionophore

Zhenhui Chen, Carmen Alcayaga, Benjamin A. Suárez-Isla, Brian O'Rourke, Gordon Tomaselli and Eduardo Marbán

J. Biol. Chem. 2002, 277:24653-24658.
doi: 10.1074/jbc.M111862200 originally published online April 24, 2002
